Kartogenin-loaded coaxial PGS/PCL aligned nanofibers for cartilage tissue engineering

João C. Silva[a,b,c], Ranodhi N. Udangawa[b], Jianle Chen[b,d], Chiara D. Mancinelli[b],
Fábio F.F. Garrudo[a,b,c], Paiyz E. Mikael[b], Joaquim M.S. Cabral[a,c], Frederico Castelo Ferreira[a,c],
Robert J. Linhardt[b,*]

[a] Department of Bioengineering and iBB - Institute for Bioengineering and Biosciences, Instituto Superior Técnico, Universidade de Lisboa, Av. Rovisco Pais, Lisboa, 1049-001, Portugal
[b] Department of Chemistry and Chemical Biology, Biological Sciences, Biomedical Engineering and Chemical and Biological Engineering, Center for Biotechnology and Interdisciplinary Studies, Rensselaer Polytechnic Institute, Troy, NY, 12180-3590, USA
[c] The Discoveries Centre for Regenerative and Precision Medicine, Lisbon Campus, Instituto Superior Técnico, Universidade de Lisboa, Av. Rovisco Pais, Lisboa, 1049-001, Portugal
[d] Ningbo Research Institute, Zhejiang University, Ningbo, 315100, China

ARTICLE INFO

ABSTRACT

Electrospinning is a valuable technology for cartilage tissue engineering (CTE) due to its ability to produce fibrous scaffolds mimicking the nanoscale and alignment of collagen fibers present within the superficial zone of articular cartilage. Coaxial electrospinning allows the fabrication of core-shell fibers able to incorporate and release bioactive molecules (e.g., drugs or growth factors) in a controlled manner. Herein, we used coaxial electrospinning to produce coaxial poly(glycerol sebacate) (PGS)/poly(caprolactone) (PCL) aligned nanofibers (core:PGS/shell:PCL). The obtained scaffolds were characterized in terms of their structure, chemical composition, thermal properties, mechanical performance and *in vitro* degradation kinetics, in comparison to monoaxial PCL aligned fibers and respective non-aligned controls. All the electrospun scaffolds produced presented average fiber diameters within the nanometer-scale and the core-shell structure of the composite fibers was clearly confirmed by TEM. Additionally, fiber alignment significantly increased (> 2-fold) the elastic modulus of both coaxial and monoxial scaffolds. Kartogenin (KGN), a small molecule known to promote mesenchymal stem/stromal cells (MSC) chondrogenesis, was loaded into the core PGS solution to generate coaxial PGS-KGN/PCL nanofibers. The KGN release kinetics and scaffold biological performance were evaluated in comparison to KGN-loaded monoaxial fibers and respective non-loaded controls. Coaxial PGS-KGN/PCL nanofibers showed a more controlled and sustained KGN release over 21 days than monoaxial PCL-KGN nanofibers. When cultured with human bone marrow MSC in incomplete chondrogenic medium (without TGF-β3), KGN-loaded scaffolds enhanced significantly cell proliferation and chondrogenic differentiation, as suggested by the increased sGAG amounts and chondrogenic markers gene expression levels. Overall, these findings highlight the potential of using coaxial PGS-KGN/PCL aligned nanofibers as a bioactive scaffold for CTE applications.

1. Introduction

Articular cartilage is a highly organized tissue comprised by four distinct zones (superficial, middle, deep and calcified zone), each with specific extracellular matrix (ECM) composition and orientation [1]. In healthy functional articular cartilage, the superficial zone consists in a very polarized dense organization of nanoscale collagen type II fibrils, which are oriented parallel to the articular surface and populated with flattened chondrocytes [2,3]. The superficial zone provides a frictionless surface to assure smooth articulation and is the main responsible for the tissue resistance to shear and tensile forces generated during movement, due to the high tensile strength provided by the aligned collagen fibers [2,4]. The age-associated wear and initial stages of osteoarthritis (OA) can lead to degradation of the collagen fibers within the superficial zone, which results in abnormal mechanical performance of the tissue and stimulates an immune response [3,5].

Electrospinning has been used in cartilage tissue engineering (CTE) applications due to its ability to fabricate fibrous scaffolds with high
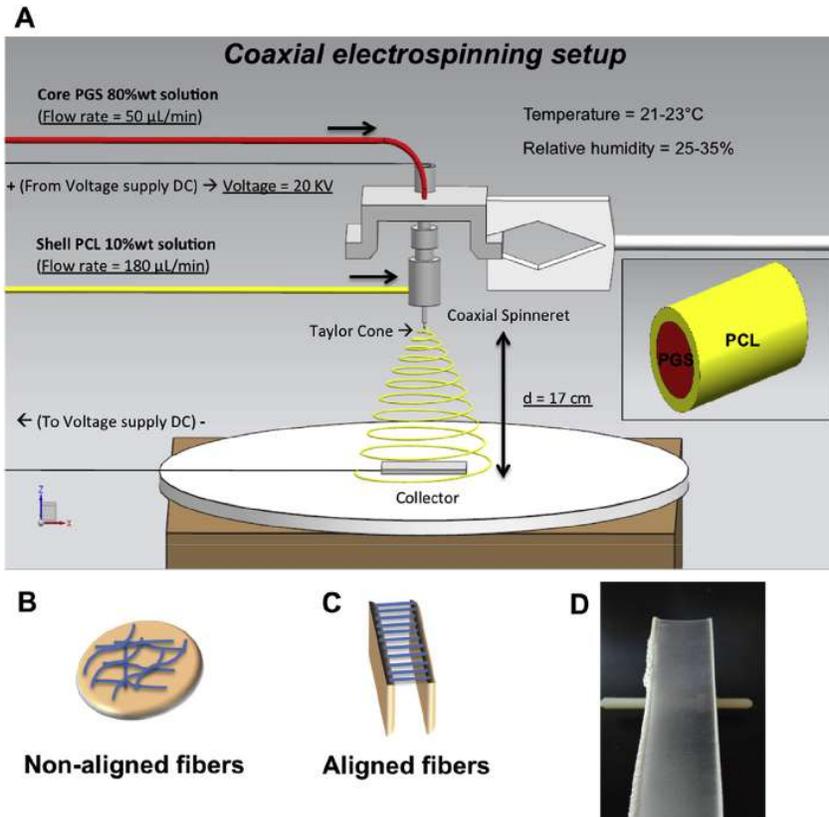

Fig. 1. Coaxial electrospinning setup and parameters used for the fabrication of coaxial aligned PGS/PCL nanofibers (A). Non-aligned nanofibers were produced in a round copper collector plate (B) and aligned nanofibers were recovered in a two parallel copper plate collector (C, D).

porosity and large surface areas mimicking the nanometer scale and alignment of the collagen fibrils present in the native articular cartilage ECM [6,7]. Coaxial electrospinning, a development of the traditional technique, uses a spinneret composed by two concentrically aligned nozzles (each one fed with a different casting solution) to fabricate fibers with a core-sheath structure. This method allows the encapsulation of nonspinnable polymers or drugs/biomolecules in the fiber core, promoting their protection and controlled-release [8]. The use of coaxial electrospun fibers in drug delivery and tissue engineering strategies has been recently reviewed [9,10]. Regarding CTE strategies, coaxial electrospun fibers incorporating growth factors have been used to enhance the chondrogenic differentiation of mesenchymal stem/stromal cells (MSC) [11–13]. In this study, coaxial aligned nanofibers with poly (glycerol sebacate) (PGS) as the core and poly(caprolactone) (PCL) as the sheath were fabricated by coaxial electrospinning.

PGS is a biodegradable and biocompatible elastomeric material, which can be easily synthesized through the polycondensation reaction of glycerol and sebacic acid, both FDA-approved [14,15]. PCL is a slow-degrading biocompatible aliphatic polyester that offers a high tensile strength, thermal stability and chemical versatility. Also, PCL has previously received FDA approval as medical implant and drug delivery device [16,17]. Both PGS and PCL have been used as scaffold materials for a wide-range of tissue engineering strategies. Importantly, PGS and PCL have also been combined to produce blended electrospun fibers for cardiac [18,19] and corneal regeneration [20]. Moreover, PCL and PGS have recently been blended to produce biomimetic porous scaffolds for CTE by salt-leaching method [21].

Kartogenin (KGN), a small heterocyclic molecule, has been described to effectively enhance the chondrogenic differentiation of human bone marrow MSC (hBMSC), exhibit chondroprotective effects

in vitro and reduce cartilage degeneration after intra-articular injection in OA mouse models [22]. KGN functions by interacting with the actin-binding protein filamin A, disrupting its balance with the transcription factor core-binding factor β (CBFβ). CBFβ enters the nucleus and interacts with RUNX1 to form the CBFβ-RUNX1 complex that activates the transcription of chondrogenesis-related proteins and enhances cartilage ECM synthesis [22,23]. In the recent years, several groups have developed biomaterial platforms to promote the sustained release of KGN towards improved cartilage and osteochondral regeneration [24–30]. However, the use of coaxial electrospun aligned fibers promoting the sustained delivery of KGN to improve cartilage regeneration is currently underexplored.

Herein, we aim to develop coaxial PGS/PCL electrospun aligned nanofibers able to promote a sustained release of KGN while being compatible with the size and alignment of native articular cartilage ECM, which might promote hBMSC chondrogenic differentiation. The electrospun scaffolds produced were characterized in terms of their structural, chemical, thermal and mechanical properties as well as for their *in vitro* biodegradation. The *in vitro* release kinetics of KGN from coaxial PGS/PCL and monoaxial PCL aligned nanofibers was evaluated for 21 days. In addition, the ability of KGN-loaded electrospun scaffolds to promote hBMSC chondrogenic differentiation in the absence of the chondrogenic cytokine transforming growth factor-beta 3 (TGF-β3) was evaluated in comparison to the respective non-loaded controls by assessing typical cartilage-ECM production and gene expression.

2. Materials and methods

2.1. Materials

Polycaprolactone (PCL, MW 80000 Da), 2,2,2-trifluoroethanol (TFE), sodium hydroxide (NaOH), dimethylsulfoxide (DMSO), isopropanol, sebacic acid and glycerol were purchased from Sigma-Aldrich (St. Louis, Missouri USA). PGS pre-polymer was synthesized based on previously reported protocols [14,31]. Briefly, sebacic acid and glycerol (in a 1:1 equimolar ratio) were reacted at 120 °C for 3 h under a nitrogen atmosphere to generate a pre-polycondensed polymer, followed by a crosslinking step at 120 °C under vacuum for 48 h. Kartogenin (KGN, MW 321.84 g/mol) was obtained from Tocris Bioscience.

2.2. Fabrication of core-shell PGS/PCL electrospun nanofibers

Polymer casting solutions for the coaxial electrospinning were prepared by dissolving PCL in TFE at 10% w/v (shell solution) and PGS in TFE at 80% w/v (core solution). The solutions were mixed overnight at room temperature to achieve homogeneity. The core-shell fibers were fabricated using an electrospinning apparatus (Fig. 1A) equipped with a coaxial spinneret (MEEC, Ogori, Fukuoka, Japan), as previously described [32]. Core PGS and shell PCL solutions were loaded into syringes placed in a mechanical syringe pump (NE-1000, New Era Pump System Inc., Wantang, NY USA) and connected by polytetrafluoroethylene (PTFE) tubing to the coaxial spinneret. The diameters of the inner and outer needles in the coaxial spinneret were 0.64 mm and 2.5 mm, respectively. The controlled flow rates of the core and shell solutions were 50 μL/min and 180 μL/min, respectively. A high voltage source (Spellman CZE1000R, Hauppauge, NY USA) was used to apply a voltage of 20 kV, creating a potential difference between the needle and copper collectors placed at a distance of 17 cm from the needle tip. Monoaxial PCL fibers were fabricated using the same process parameters, with a needle with 0.64 mm diameter and a flow rate of 180 μL/min. The non-aligned and aligned electrospun fibers were produced on different collectors: a round copper plate (Fig. 1B) for non-aligned fibers and a two parallel copper plates (separated by 2 cm) collector (Fig. 1C) was used to align fibers. All the fiber groups were produced under similar ambient conditions (temperature and relative humidity varied between 21-23 °C and 25–35%, respectively). Prior to further use, the fibers were dried in a desiccator to remove any remaining solvents.

2.3. Characterization of coaxial PGS/PCL electrospun nanofibers

2.3.1. Scanning electron microscopy (SEM) analysis

The structural characterization of the non-aligned/aligned coaxial PGS/PCL and monoxial PCL fibers was performed using a field emission scanning electron microscope (FE-SEM, FEI-Versa 3D Dual Beam, Hillsboro). Prior to imaging, samples were mounted on a holder using carbon tape and sputter-coated with a thin layer of gold-palladium (60:40). Samples were imaged at several magnifications using an accelerating voltage of 3–5 kV. The average fiber diameters and subsequent distributions of both non-aligned/aligned coaxial PGS/PCL and monoaxial PCL electrospun scaffolds were determined by measuring 100 individual fibers per condition from at least 5 different SEM images using the ImageJ software (ImageJ 1.51f, National Institutes of Health, USA). Additionally, the mats were cross-sectioned in liquid nitrogen, mounted and sputter-coated, and imaged by SEM to assess the core-shell structure of the fibers.

2.3.2. Transmission electron microscopy (TEM) analysis

The core-shell nature of coaxial PGS/PCL electrospun fibers was confirmed by transmission electron microscopy (TEM). The coaxial PGS/PCL fibers were spun directly on lacey carbon coated 200 mesh copper grids and imaged using a JEOL-JEM-2011 TEM (JEOL Ltd.,

Tokyo, Japan) operating at an accelerating voltage of 200 kV.

2.3.3. X-ray diffraction (XRD) analysis

X-ray diffraction (XRD) analysis was used to confirm the presence of both PCL and PGS materials in the coaxial PGS/PCL electrospun fibers. Thus, coaxial PGS/PCL and monoaxial PCL fiber mats as well as PGS and PCL raw polymers were evaluated using a Bruker D8-DISCOVER X-ray diffractometer equipped with a $Cu_{K\alpha}$ radiation source and a pyrolytic graphite monochromator.

2.3.4. ATR-FTIR analysis

A Spectrum One FTIR Spectrometer (PerkinElmer, USA) working in the Attenuated total reflectance – Fourier transform infrared (ATR-FTIR) mode was used to collect the spectra of both coaxial PGS/PCL and monoaxial PCL electrospun fibers in the spectral region 4000-650 cm^{-1} and with a resolution of 4 cm^{-1}. Characteristic peaks were identified by comparison with the spectra of PCL and PGS raw polymers.

2.3.5. Differential scanning calorimetric (DSC) analysis

Pre-weighed samples of coaxial PGS/PCL fibers, monoaxial PCL fibers and respective PCL, PGS raw polymers were hermetically sealed in aluminum pans and submitted to healing and cooling cycles between −50 °C and 100 °C at a constant heating rate of 5 °C/min using a TA Instruments DSC-Q100 equipment (New Castle, Delaware USA) under nitrogen supply. The thermal properties of the samples, namely the melting and crystallization temperatures were determined using the Universal Analysis software V4.7A (TA Instruments).

2.3.6. Mechanical tensile testing

The mechanical properties of non-aligned/aligned monoaxial PCL and coaxial PGS/PCL electrospun scaffolds were assessed under uniaxial tensile testing using a mechanical tester (Instron® Model 5544) with a 10 N load cell and a constant displacement rate of 10 mm/min. For each condition, five different test specimens (n = 5) were prepared in a rectangular shape with a length of 15 mm, width of 10 mm and a thickness of 0.2 mm. Bluehill® 2 software was used to collect and process the experimental data from the tensile tests. Young's elastic moduli were calculated from the initial 0–15% linear in the stress-strain curve. Ultimate tensile strength (UTS) was measured from the highest peak of the stress-strain curves.

2.3.7. In vitro accelerated degradation assay

Monoaxial PCL and coaxial PGS/PCL electrospun mats were cut into 15 mm × 7 mm x 0.2 mm and subjected to an accelerated degradation assay by incubation with 5 mL of 0.5 mM NaOH solution in PBS (Gibco) at 37 °C for different time periods (7, 14 and 21 days). Upon incubation at each degradation time point, electrospun scaffolds were rinsed gently with PBS and dried under vacuum. The sample weight (*Wt*) (n = 3) was measured and the percentage of weight loss was determined by dividing the obtained weight loss to the initial dry weight (*Wo*) of each sample before incubation ([(*Wo-Wt*)/*Wo*] x 100).

2.4. In vitro kartogenin (KGN) release assay

KGN was dissolved in a mixture of DMSO:TFE (volume ratio 20:80) under agitation overnight and then combined with the polymer casting solutions at a final concentration of 2 mg/mL to fabricate two different groups of aligned electrospun fibers following the procedure described in subsection 2.2: coaxial PGS-KGN/PCL (core solution: PGS 80%-KGN 0.2% w/v and shell solution: PCL 10% w/v) and monoaxial PCL-KGN (solution: PCL 10%-KGN 0.2% w/v). KGN-loaded electrospun scaffolds (15 mm × 7 mm x 0.2 mm) were weighed, immersed in 1 mL of PBS (pH 7.4) and placed on a shaker (100 rpm) at 37 °C with a humidified atmosphere to mimic physiological conditions. At each sampling time, the total volume of PBS was collected and replaced with the same volume of fresh PBS to determine the release kinetics of KGN from the

electrospun scaffolds. The amount of KGN released from each electrospun scaffold was evaluated using HPCL (Agilent 1200 LC system, EC-C18 reverse phase column) and normalized to the scaffold initial weight. *In vitro* release was measured from five scaffolds (n = 5) at different time-points during 21 days (0, 1, 3, 6, 12, 24, 48, 72, 120, 168, 216, 288, 360, 432 and 504 h).

2.5. hBMSC seeding and culture on KGN-loaded electrospun aligned nanofibers

Prior to cell seeding, the electrospun scaffolds were sterilized by UV exposure for 3 h, placed in ultra-low cell attachment 24-well plates and washed three times with PBS + 1% penicillin-streptomycin (Pen-Strep, Gibco) solution. Afterwards, the scaffolds were soaked in culture medium and incubated at 37 °C for 1 h.

Human bone marrow MSC (hBMSC) were purchased from Lonza (Basel-Switzerland), thawed and expanded on tissue culture flasks (CELLTREAT® Scientific Products, MA) using low-glucose Dulbecco's Modified Eagle Medium (DMEM, Gibco, Grand Island, NY) supplemented with 10% fetal bovine serum (FBS, Gibco) and 1% Pen-strep, and kept at 37 °C and 5% CO_2 in a humidified atmosphere until scaffold seeding. Complete medium renewal was performed every 3–4 days and all the experimental assays were performed using cells in passage 3 or 4.

hBMSC were seeded on the electrospun nanofiber scaffolds at a density of 50000 cells/scaffold and incubated for 2 h at 37 °C and 5% CO_2 without culture medium to favor initial cell attachment. Afterwards, incomplete chondrogenic medium composed by high glucose DMEM (Thermo Fisher Scientific) with 100 nM dexamethasone (Sigma-Aldrich), 50 μg/mL ascorbic acid 2-phosphate (Sigma-Aldrich), 40 μg/mL L-proline (Sigma-Aldrich), 1 mM sodium pyruvate (Gibco), ITS™ + Premix supplement (6.25 μg/mL bovine insulin; 6.25 μg/mL transferrin; 6.25 μg/mL selenous acid; 5.33 μg/mL linoleic acid; 1.25 μg/mL BSA, Corning), Pen-strep (100 U/mL penicillin; 100 μg/mL streptomycin) was added to all the scaffolds. The cultures were conducted during 21 days at 37 °C and 5% CO_2 under low oxygen conditions (5% O_2-mimicking the hypoxic environment of articular cartilage) and the culture medium (without TGF-β3) was fully renewed every 3–4 days.

2.6. Evaluation of the biological performance and chondrogenic potential of KGN-loaded aligned electrospun nanofibers

2.6.1. hBMSC proliferation assay
The proliferation of hBMSC on the monoaxial/coaxial KGN-loaded aligned nanofibers and respective controls was evaluated using AlamarBlue® cell viability reagent (ThermoFischer Scientific, USA) on days 3, 7, 14 and 21 following the manufacturer's guidelines. Briefly, a 10% (v/v) AlamarBlue® solution in culture medium was added to the scaffolds and incubated at 37 °C in 5% CO_2 chamber for 3 h. Fluorescence intensity was quantified in a microplate reader (SpectraMax M5, Molecular Devices, USA) at an excitation/emission wavelength of 560/590 nm. The obtained fluorescence intensity values were correlated to the equivalent number of viable cells present in each scaffold through a calibration curve. Three independent scaffolds (n = 3) were analyzed per condition and the fluorescence values of each sample were measured in triplicate. For each experimental group, acellular electrospun scaffolds were used as blank controls.

2.6.2. Cell morphology assessment by SEM
The morphology of the cells cultured for 21 days on the monoaxial/coaxial KGN-loaded aligned nanofibers and respective controls was observed by SEM. The scaffold samples were fixed with 4% PFA for 20 min, stained with 1% (v/v) osmium tetroxide (Sigma-Aldrich) solution for 30 min and washed twice with PBS. Afterwards, samples were dehydrated using ethanol gradient solutions (20%, 40%, 60%, 80%,

95% and 100% (v/v)) for 20 min each and finally dried in a critical point dryer (supercritical Automegasamdri 915B, Tousimis, USA) in 100% isopropanol. Dried samples were mounted, sputter-coated and imaged using the above-mentioned SEM procedure (subsection 2.3.1.).

2.6.3. sGAG content quantification (DMMB assay)
At days 14 and 21 of differentiation, the electrospun scaffolds were collected, washed with PBS, and digested in a 125 μg/mL papain enzyme (from papaya latex, Sigma-Aldrich) solution (50 mM sodium phosphate, 2 mM N-acetyl cysteine, 2 mM EDTA, all from Sigma-Aldrich, pH 6.5) at 60 °C overnight (16–18 h). The sulfated glycosaminoglycans (sGAG) produced by cells on the electrospun scaffolds were quantified using 1,9-dimethylmethylene blue (DMMB, Sigma-Aldrich) assay. The digested samples were mixed with a DMMB solution (16 mg DMMB in 0.3% w/v glycine, 0.27% sodium chloride in distilled water, pH 3.0) in 96-well plates and the absorbance was measured at 525 nm. The sGAG amounts were extrapolated from a calibration curve generated using chondroitin 6-sulfate (sodium salt from shark cartilage, Sigma-Aldrich) standards and normalized to the number of cells present in each scaffold. Three scaffolds (n = 3) were used for each experimental group and the absorbance values were measured in triplicate. Acellular electrospun scaffolds for each experimental group were used as blank controls.

2.6.4. RNA isolation and quantitative real time PCR (RT-qPCR) analysis
Total RNA was extracted from the final constructs (day 21) using the RNeasy Mini Kit (QIAGEN, Hilden, Germany). The samples were incubated in lysis buffer with 200 rpm agitation for 30 min at 4 °C and total RNA was isolated according to the manufacturer's protocol. Isolated RNA was quantified using a Nanodrop (ND-100 Spectrophotometer, Nanodrop Technologies). cDNA was synthesized from the purified RNA using iScript™ Reverse Transcription Supermix (Bio-Rad, Hercules, CA USA) following the manufacturer's guidelines. The reaction mixtures were incubated in a thermal cycler (Veriti Thermal Cycler, Applied Biosystems, CA USA) with the following temperature protocol: 5 min at 25 °C, 20 min at 46 °C and 1 min at 95 °C, and then maintained at 4 °C.

Real time quantitative reverse transcription-polymerase chain reaction (RT-qPCR) analysis was performed using the TaqMan® Fast Advanced Master Mix (Applied Biosystems) and StepOnePlus real-time PCR system (Applied Biosystems) according to the manufacturer's protocol. Reactions were run in triplicate using the TaqMan® Gene Expression Assays (20X) (Thermo Fisher Scientific) presented in Supplementary Table 1. The CT values obtained were normalized against the expression of the housekeeping gene *GAPDH* and the analysis was performed using the $2^{-\Delta\Delta Ct}$ method. Results for target gene expressions in the different experimental groups are presented as fold-change expression levels relative to hBMSC before scaffold seeding (day 0).

2.6.5. Immunofluorescence analysis
After 21 days of differentiation, the medium was removed and the electrospun scaffolds were washed with PBS and fixed with PFA 4% for 20 min. The samples were then washed twice with PBS, and permeabilized and blocked with a solution of 0.3% Triton X-100 (Sigma-Aldrich), 1% BSA (Sigma-Aldrich) and 10% Goat serum (ThermoFischer Scientific) in PBS at room temperature for 30 min. A solution containing primary antibody for collagen II (1:200 in blocking solution, mouse collagen II monoclonal antibody 6B3, ThermoFisher Scientific) was incubated with the samples overnight at 4 °C. Afterwards, the samples were washed once with 1% BSA solution (in PBS) and incubated with the secondary antibody Goat anti-mouse IgG AlexaFluor 488 (1:150 in 1% BSA (in PBS) solution, ThermoFisher Scientific) for 1 h at room temperature and protected from light. Finally, the scaffolds were counterstained with DAPI (Sigma-Aldrich) for 5 min at room temperature, washed with PBS and imaged using a confocal microscope (Zeiss
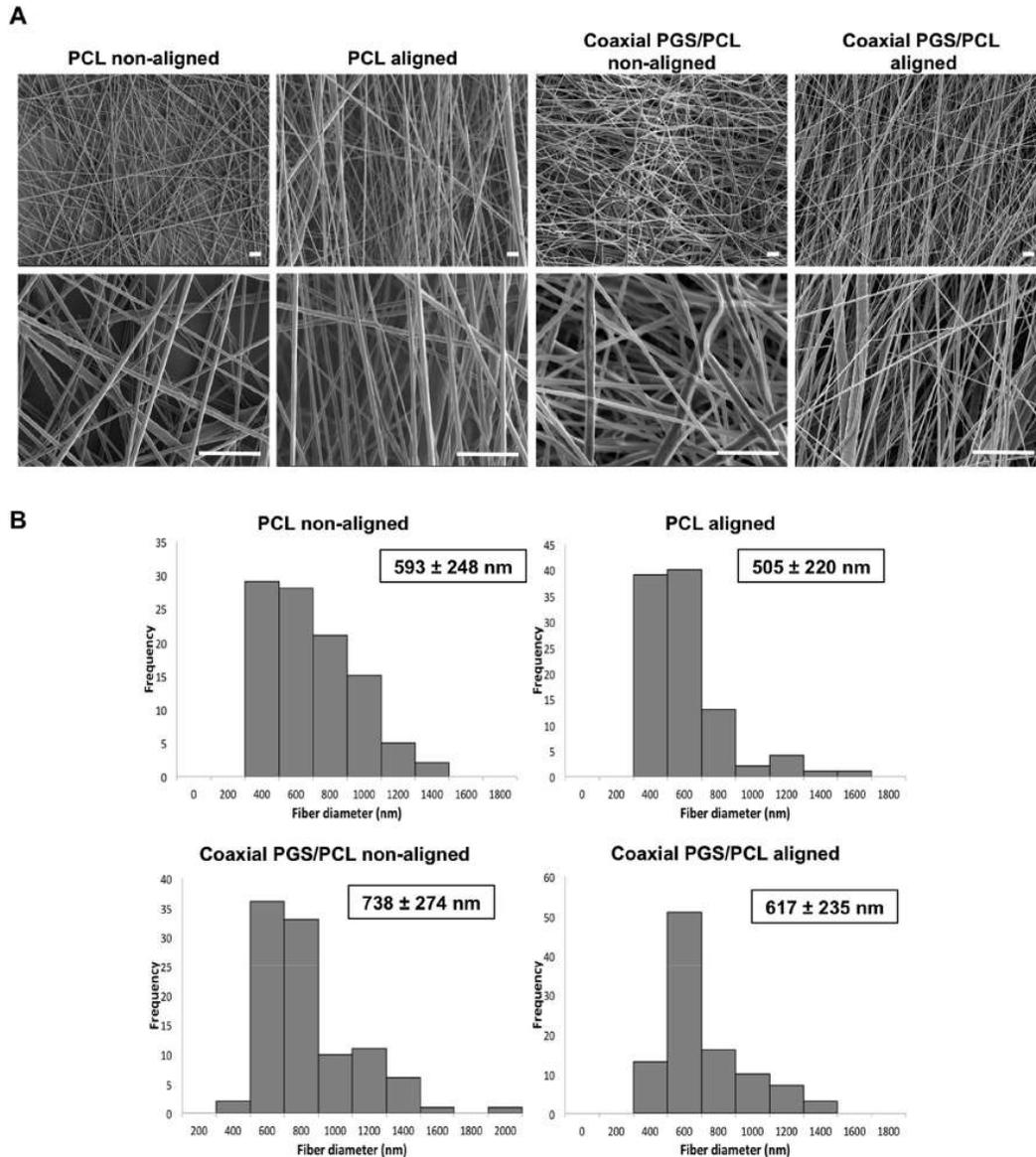
Fig. 2. SEM images (at two different magnifications) of the non-aligned/aligned monoaxial PCL and coaxial PGS/PCL nanofibers (A) and respective fiber diameter distribution histograms (B). Scale bar: 5 μm.

LSM 510META Spectral Confocal).

2.7. Statistical analysis

Results are presented as mean values ± standard deviation (SD). Each experiment was conducted in triplicate (n = 3), unless specified differently. The statistical analysis of the data was performed using one-way ANOVA, followed by Tukey post-hoc test. GraphPad Prism version 7 software was used in the analysis and data was considered to be significant when p-values obtained were less than 0.05 (95% confidence intervals, *$p < 0.05$).

3. Results

3.1. Coaxial PGS/PCL electrospun nanofibers structural characterization

Coaxial PGS/PCL and monoaxial PCL aligned nanofibers as well as

their respective non-aligned controls were analyzed by SEM. SEM micrographs (Fig. 2A) showed that all the electrospun scaffolds were highly porous and interconnected, which favors oxygen and media diffusion through the scaffold and provides an adequate surface area for cell adhesion. Fig. 2B shows the average fiber diameter and respective distributions for all conditions studied. It should be noted that all the electrospun scaffolds presented average fiber diameters in the nanometer scale (505–738 nm), which is advantageous to mimic the structural features of *in vivo* articular cartilage ECM. Interestingly, both coaxial PGS/PCL and monoaxial PCL aligned nanofibers presented slightly decreased average fiber diameters than their non-aligned counterparts. The core-shell structure of the fibers was confirmed by TEM (Fig. 3), as it is possible to clearly distinguish between the two different materials, PGS in the core and PCL in the shell (Fig. 3B), as opposed to PCL monoaxial fiber (Fig. 3A). The coaxial structure was also observed by SEM analysis of cross-sectioned fibers (Fig. 3C).
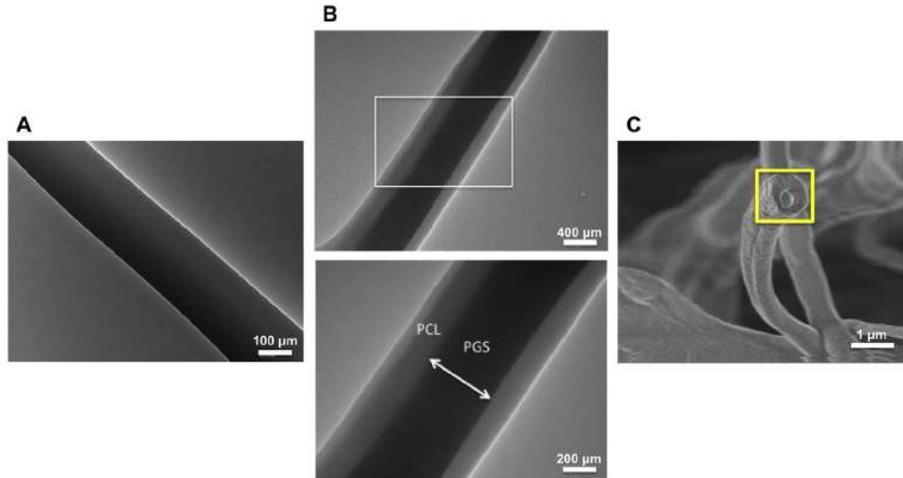
Fig. 3. Confirmation of the core-shell structure of the produced coaxial electrospun nanofibers. TEM images of monoaxial PCL nanofibers (A) and of coaxial PGS/PCL aligned nanofibers (B). The bottom image in B corresponds to a magnification of the top image (white box). The core-shell structure of coaxial PGS/PCL nanofibers was further confirmed by SEM analysis of cross-sectioned fibers, highlighted by the yellow box (C). Scale bars are depicted in the figure. (For interpretation of the references to colour in this figure legend, the reader is referred to the Web version of this article.)

3.2. Chemical, thermal, mechanical and degradation properties of coaxial PGS/PCL electrospun nanofibers scaffolds

The chemical characterization of the coaxial PGS/PCL nanofibers in comparison with PCL nanofibers as well as with the PGS pre-polymer and pure PCL polymer was performed by XRD (Fig. 4A) and FTIR analysis (Fig. 4B). XRD spectra of both PCL polymer and nanofibers show the presence of two peaks at 21.3° and 23.7°, while the PGS polymer exhibits two peaks at 19.3° and 23°. The XRD spectra for the coaxial PGS/PCL nanofibers present three peaks including the two major peaks of the PCL spectra and a peak at 19.3° that can be assigned to the PGS portion, thereby confirming the presence of both PCL and PGS polymers in their constitution.

The presence of both PGS and PCL in the coaxial electrospun scaffolds was also confirmed by FTIR analysis. Both PGS and PCL (polymer and nanofibers) showed very similar major IR peaks at approximately $2943\,cm^{-1}$ (CH_2 stretching-asymmetric), $2864\,cm^{-1}$ (CH_2 stretching-symmetric), $1725\,cm^{-1}$ (ester carbonyl bond stretching) and $1187\,cm^{-1}$ (carbon-oxygen bond stretching). Despite being slightly masked by the other peaks higher amplitude, the PGS spectra showed an additional hydroxyl group peak at $3450\,cm^{-1}$, which was not present in PCL. The coaxial PGS/PCL nanofibers presented all the mentioned peaks, confirming the composite nature of the fibers.

The thermal properties of the fabricated electrospun scaffolds were assessed using DSC analysis (Supplementary Fig. 1). DSC thermograms of heating (Supplementary Fig. 1A) and cooling (Supplementary

Fig. 1B) cycles for the electrospun scaffolds and respective individual polymers also supported the composite nature of the coaxial nanofibers. As expected, the coaxial PGS/PCL nanofibers exhibit two distinct melting temperatures (T_m) ($T_{m\text{-}PCL} = 52.90\,°C$ and $T_{m\text{-}PGS} = 13.45\,°C$) and crystallization temperatures (T_c) ($T_{c\text{-}PCL} = 27.28\,°C$ and $T_{c\text{-}PGS} = -7.77\,°C$) indicating the presence of both polymers in its constitution. All the melting and crystallization temperatures calculated are summarized in Supplementary Fig. 1C.

The analysis of the mechanical properties of the electrospun scaffolds under tensile testing is shown in Fig. 5. Coaxial and monoaxial non-aligned nanofibers were also considered in the analysis to assess the effect of fiber alignment on the scaffold's mechanical performance. Representative stress-strain curves for all the conditions tested are presented in Fig. 5A. Fiber alignment resulted in a significant increase ($p < 0.05$) in the elastic modulus in both monoaxial (9.90 ± 0.87 MPa in PCL aligned compared to 4.02 ± 0.88 MPa in PCL non-aligned) and coaxial (11.78 ± 0.73 MPa in coaxial PGS/PCL aligned compared 5.06 ± 1.51 MPa in coaxial PGS/PCL non-aligned) configurations. It is also possible to observe that the addition of PGS in the core of coaxial fibers resulted in an increase in the elastic modulus when compared to the respective monoaxial counterparts, however, such increase was not statistically significant (Fig. 5B). Regarding the UTS, aligned fibers also presented higher values than the non-aligned counterparts, however significant differences were only observed for monoaxial PCL fibers (Fig. 5C).

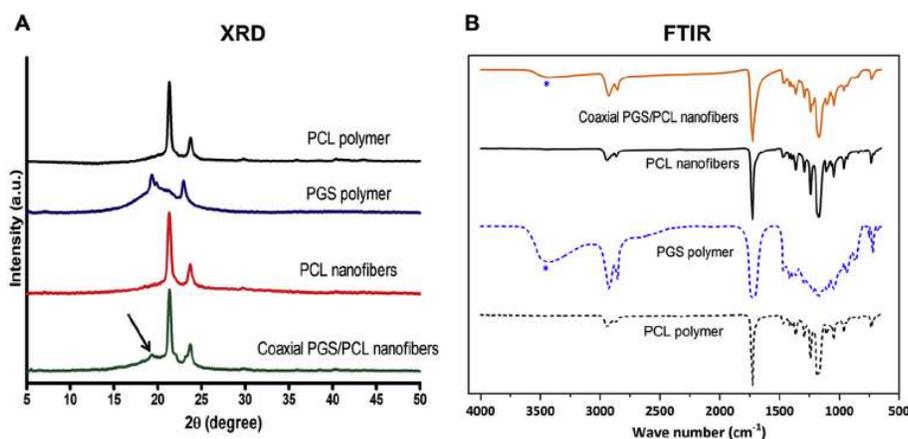The degradation of coaxial PGS/PCL and monoaxial PCL aligned

Fig. 4. XRD (A) and FTIR (B) analysis of coaxial PGS/PCL nanofibers, monoxial PCL nanofibers and respective PGS and PCL polymers. The black arrow and blue asterisk highlight the characteristic peaks that allowed confirm the presence of both PCL and PGS in the coaxial electrospun nanofibers. (For interpretation of the references to colour in this figure legend, the reader is referred to the Web version of this article.)
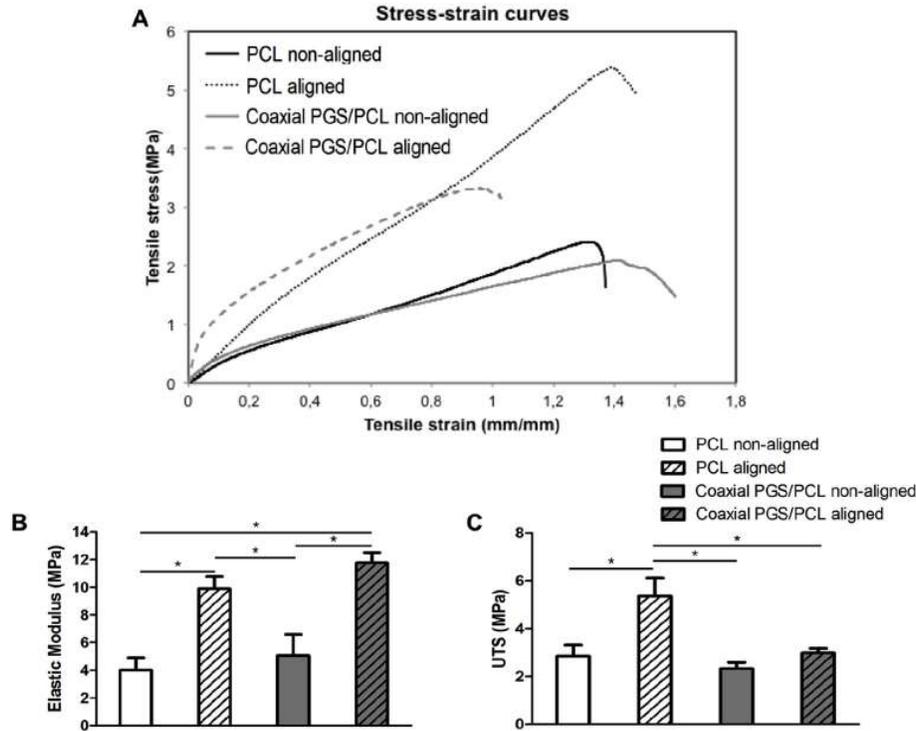
Fig. 5. Mechanical properties of aligned/non-aligned monoaxial PCL and coaxial PGS/PCL electrospun scaffolds: representative stress-strain curves (A), elastic modulus (B) and ultimate tensile strength (UTS) (C). Five independent specimens were used in the analysis (n = 5). *p < 0.05.

electrospun scaffolds was studied under accelerated conditions (in 0.5 mM NaOH solution) for 21 days (Supplementary Fig. 2). After 21 days, monoaxial PCL electrospun scaffolds showed only a residual mass loss (2.3 ± 1.4%), confirming the reported slow-degradation behavior of the PCL polymer. In contrast, coaxial PGS/PCL nanofibers showed a higher degradation rate, reaching a weight loss of 23 ± 1.6% at the end of the experiment (Supplementary Fig. 2A). This is in accordance with SEM images of the samples taken before (day 0) and after the accelerated degradation assay (day 21), in which a considerable deterioration of the fibers was observed in coaxial PGS/PCL electrospun scaffolds (Supplementary Fig. 2B).

3.3. KGN release profile from coaxial PGS-KGN/PCL and monoaxial PCL-KGN aligned nanofibers

KGN (Fig. 6B) was loaded into the core PGS solution to produce coaxial PGS-KGN/PCL aligned nanofibers and also into the PCL solution to generate monoaxial PCL-KGN aligned nanofibers (Fig. 6A). The addition of KGN did not result in any meaningful changes on the structural and mechanical properties of the nanofibrous scaffolds fabricated. The produced scaffolds were assessed for the *in vitro* release kinetics of KGN during 21 days. For both scaffold types, the KGN release profile was characterized by an initial burst release until 24 h, followed by a relatively slow and nearly linear release. As it is possible to observe in Fig. 6C, coaxial nanofibers allowed a much more sustained release and an alleviated burst release than the monoaxial nanofibers. During the 21 days of the *in vitro* study, a total of 0.32 ± 0.03 µg KGN/mg of scaffold and 1.11 ± 0.44 µg KGN/mg of scaffold were released from the coaxial PGS-KGN/PCL and monoaxial PCL-KGN nanofibers, respectively.

3.4. Effects of KGN-loaded electrospun nanofibers on cell proliferation and morphology

The effects of KGN release on hBMSC proliferation (Alamar Blue assay) were evaluated *in vitro* using both coaxial PGS-KGN/PCL and monoaxial PCL-KGN aligned nanofibers in comparison to non-loaded controls (Fig. 7A). At the end of the experiment (day 21), both coaxial PGS-KGN/PCL and monoaxial PCL-KGN aligned nanofibers showed significantly higher (p < 0.05) equivalent cell numbers than the scaffolds without KGN. The coaxial PGS-KGN/PCL electrospun scaffolds also showed improved hBMSC proliferation in comparison to monoaxial PCL-KGN ones, however, such increase was not statistically significant. Interestingly, the coaxial PGS-KGN/PCL scaffolds presented a significantly enhanced hBMSC proliferation in comparison with non-loaded coaxial PGS/PCL scaffolds since earlier stages of the culture (from day 7 onwards). The morphology of hBMSCs on the different electrospun scaffolds was evaluated after 21 days by SEM analysis (Fig. 7B).

3.5. hBMSC chondrogenic differentiation on KGN-loaded electrospun nanofibers

The ability of KGN-loaded coaxial and monoaxial electrospun scaffolds to promote hBMSC chondrogenesis was evaluated by assessment of cartilage-like ECM production and of chondrogenic gene markers expression. As shown in Fig. 8, all the scaffolds tested supported sGAG production (Fig. 8A) over time and stained positively for the presence of collagen II (Fig. 8B), both main components of articular cartilage ECM. At day 14, higher amounts were observed for PCL-KGN electrospun scaffolds (7.92 ± 1.32 µg sGAG/10^5 cells) compared to all other groups. After 21 days of chondrogenic differentiation, PCL, PCL-KGN, coaxial PGS/PCL and coaxial PGS-KGN/PCL electrospun scaffolds afforded sGAG amounts of 7.50 ± 1.96 µg/10^5 cells, 9.74 ± 1.93 µg/
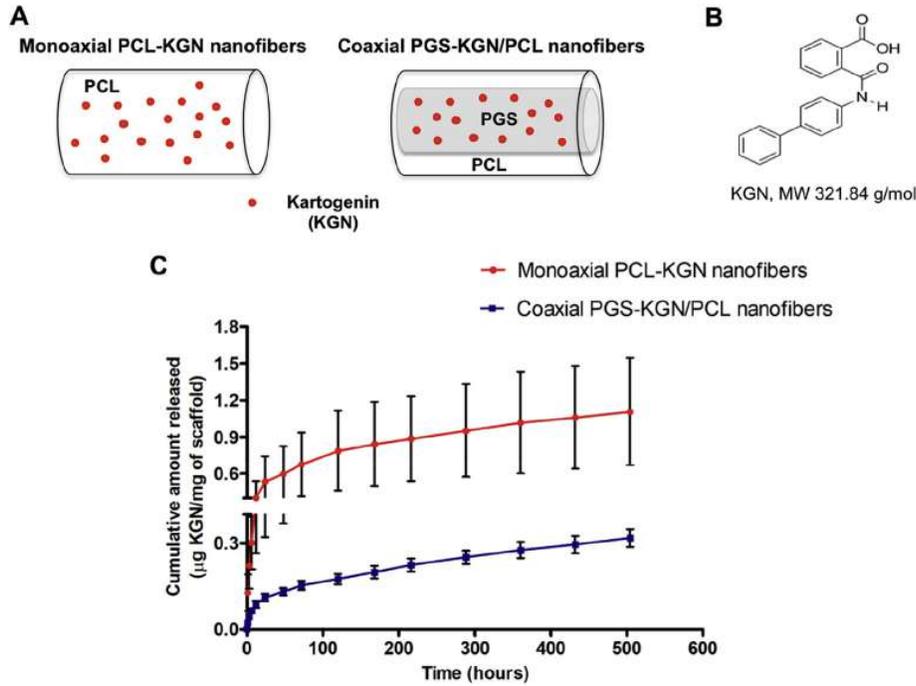
Fig. 6. *In vitro* release kinetics of KGN from coaxial PGS-KGN/PCL and monoaxial PCL-KGN aligned nanofibers for 21 days at 37 °C, pH = 7.4 and 100 rpm: schematic representation of the coaxial PGS-KCN/PCL and monoaxial PCL-KGN fibers (A), chemical structure of KGN (B), and cumulative amount of KGN released as a function of time and normalized to the weight of the scaffold. Results are presented as mean ± SD of five independent scaffolds (n = 5).

10^5 cells, 5.09 ± 2.04 µg/10^5 cells and 10.12 ± 1.91 µg/10^5 cells, respectively. Despite the fact that both KGN-loaded scaffolds afforded higher amounts of sGAG than the scaffolds without KGN, a statistically significant ($p < 0.05$) enhancement was just observed for the coaxial PGS-KGN/PCL scaffolds compared to non-loaded counterparts.

Gene expression in the different groups of electrospun nanofiber scaffolds tested was evaluated at the end of the differentiation protocol

(day 21) by RT-qPCR analysis (Fig. 9). All the scaffolds showed no significant upregulation of *COL1A1* gene (Fig. 9A), a fibrocartilage marker, in comparison to the control (hBMSC at day 0). KGN-loaded electrospun scaffolds demonstrated significantly higher ($p < 0.05$) expressions of *COL2A1* (Fig. 9B), *Sox9* (Fig. 9C) and *ACAN* (Fig. 9D) genes in comparison to the non-loaded scaffolds. Moreover, no statistically significant differences were observed between coaxial PGS-KGN/
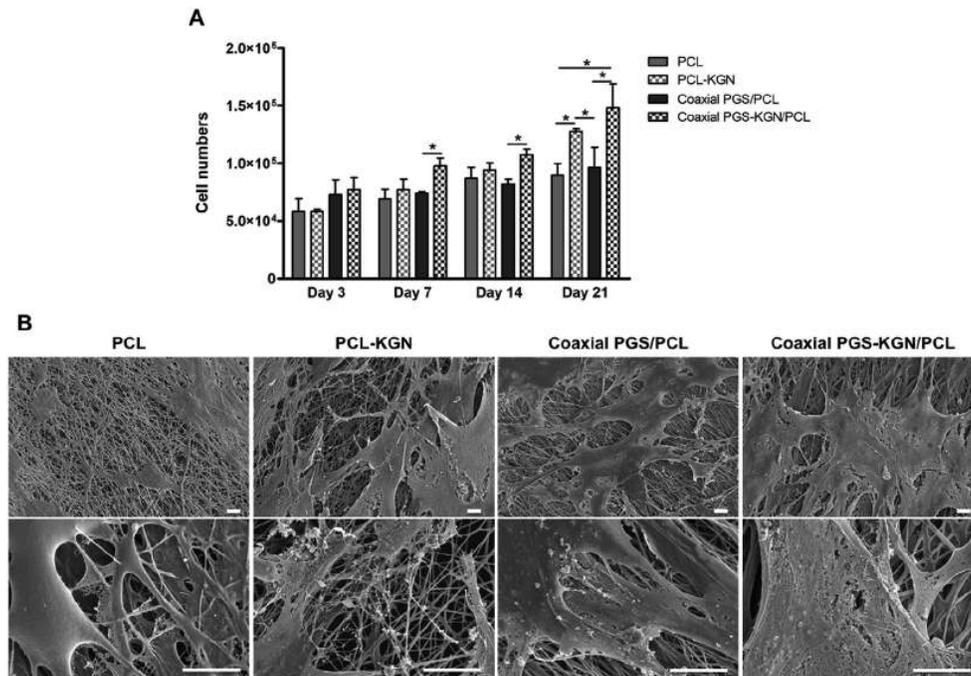

Fig. 7. Effects of KGN-loaded monoaxial and coaxial aligned nanofibers on hBMSC proliferation and morphology: Cell proliferation assay (A) and SEM images showing hBMSC morphology on all the electrospun scaffolds tested (at day 21) (B). Results are presented as mean ± SD (n = 3). *$p < 0.05$. Scale bar: 10 µm.
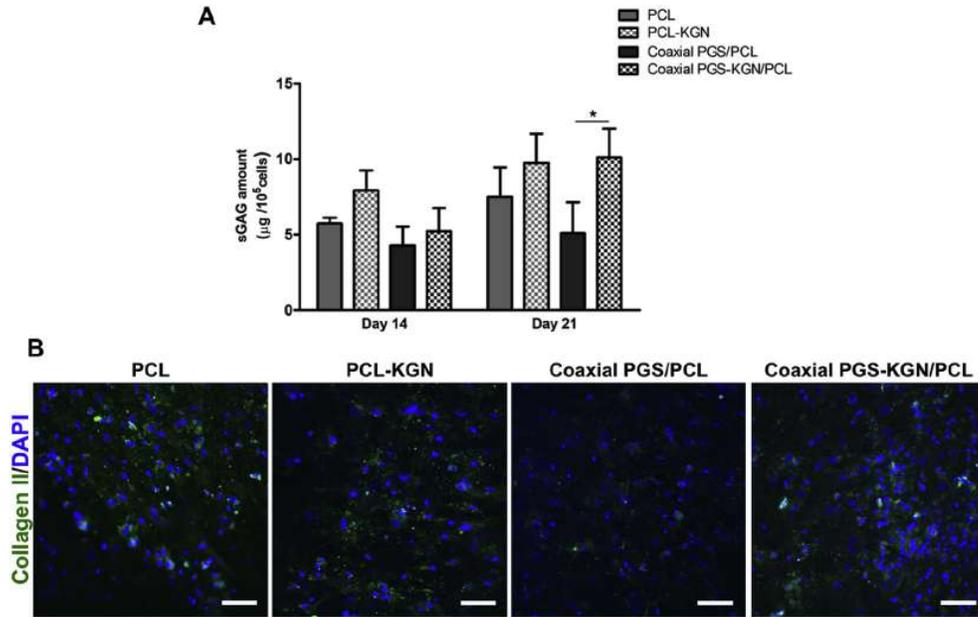
Fig. 8. Effects of KGN-loaded monoaxial and coaxial aligned nanofibers on cartilage ECM production: sGAG amounts produced after 14 and 21 days (A) and immunofluorescence analysis to evaluate the presence of collagen II on the electrospun scaffolds (at day 21) (B). For immunofluorescence staining, samples were counterstained with DAPI. Results are presented as mean ± SD (n = 3). *$p < 0.05$. Scale bar: 50 μm.
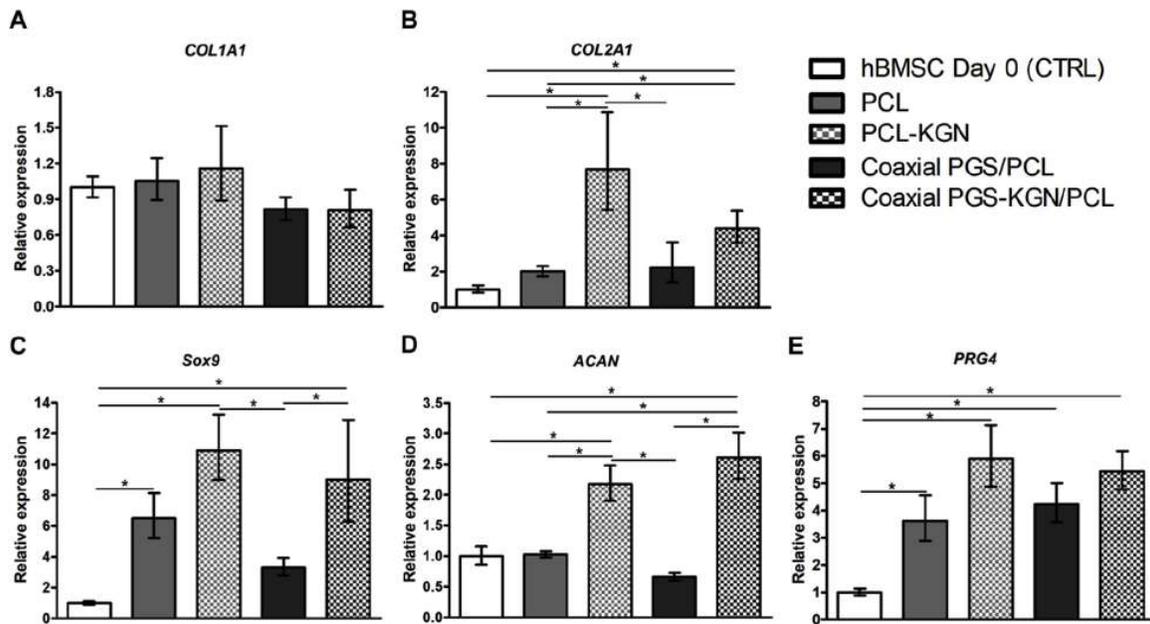

Fig. 9. Effects of KGN-loaded monoaxial and coaxial aligned nanofibers on the gene expression of hBMSC evaluated by RT-qPCR after 21 days of chondrogenic differentiation. Expressions of *COL1A1* (A), *COL2A1* (B), *Sox9* (C), *ACAN* (D) and *PRG4* (E) were normalized to *GAPDH* and calculated as a fold-change relative to the baseline expression of the control sample (hBMSC before scaffold seeding at day 0). Results are presented as mean ± SD; n = 3; *$p < 0.05$.

PCL and monoaxial PCL-KGN electrospun scaffolds. It is noteworthy that all the electrospun scaffolds resulted in significant upregulation of the PRG4 gene (Fig. 9E), which encodes for lubricin/superficial zone protein (SZP) present in the superficial layer of articular cartilage and responsible for lubrication at the joint surface.

4. Discussion

The fabrication of biomimetic scaffolds recreating the structural features of articular cartilage ECM is crucial for successful tissue regeneration. Biodegradable electrospun nanofiber scaffolds have been extensively explored in combination with MSC for CTE applications [7,33–35]. Synthetic polymers are commonly used to produce electrospun scaffolds for CTE due to their versatility, superior mechanical

properties and higher consistency across batches [36]. Despite PGS emergence as a promising scaffold material for a variety of tissue engineering applications, processing of PGS prepolymer into stable fibrous scaffolds by electrospinning is challenging due to its low molecular weight and subsequent low solution viscosity even at high concentrations [37]. Strategies used to overcome this limitation include blending with other synthetic or natural materials or the adoption of coaxial fiber configuration, encapsulating PGS in the core [38–41]. Remarkably, in a recent study, Wu and colleagues reported the production of microfibrous membranes solely composed of PGS by combining coaxial electrospinning with an additional curing step and subsequent removal of the shell material [42].

In this study, we used coaxial electrospinning to fabricate core-shell PGS/PCL aligned nanofiber scaffolds able to mimic the structural features of cartilage ECM, promote the delivery of a chondroinductive small molecule and support cell culture. All the electrospun scaffolds produced were comprised of fibers in the nanometer scale, which was previously shown to be advantageous for MSC chondrogenic differentiation [7,43]. Schagemann and colleagues observed enhanced hBMSC chondrogenic differentiation in PCL nanofibrous scaffolds with fiber diameters of approximately 400 nm in comparison to PCL microfibrous scaffolds [43]. The core-shell structure of the coaxial PGS/PCL scaffolds produced was clearly observed by SEM and TEM. The composite nature of the coaxial fibers produced was further confirmed by XRD, FTIR and DSC analysis, which was in accordance with previously reported characterizations [44,45].

The coaxial PGS/PCL aligned nanofibrous scaffolds had an elastic modulus of approximately 11.8 ± 0.7 MPa, which is slightly higher, but close to values previously reported for PGS-PCL blend aligned scaffolds [18,44]. We observed that the core-shell configuration of the coaxial fibers presented a much lower effect on the electrospun scaffold's elastic modulus than fiber alignment. In fact, coaxial PGS/PCL and monoaxial PCL aligned nanofiber scaffolds showed 2.3-fold and 2.5-fold higher elastic modulus than their respective non-aligned counterparts. This is corroborated by a previous work, in which it was reported that aligned PCL scaffolds afforded a 2.2-fold higher elastic modulus compared to randomly oriented scaffolds [46]. Additionally, Gaharwar et al. also observed similar behavior for aligned PGS-PCL blend microfibrous scaffolds [44]. Importantly, our coaxial PGS/PCL scaffold had an elastic modulus under tensile testing within the range of the tensile modulus described for healthy cartilage (5–25 MPa), which varies considerably based on tissue location as result of zonal collagen distribution [2]. In addition, as previously reported by Hou and colleagues for non-aligned coaxial PGS/PCL electrospun microfibers, there is an advantageous possibility of tuning the scaffolds mechanical properties by varying the amount of PGS present in the fiber core [40].

The degradation of both coaxial PGS/PCL and monoaxial PCL aligned nanofibers was evaluated *in vitro* for 21 days under accelerated hydrolytic conditions. PCL and PGS have considerably different biodegradation rates. While the fast degrading PGS is reported to be completely resorbed in the body within 60 days, PCL has a resident time *in vivo* of more than 2 years [47,48]. Accordingly, Masoumi et al. showed that the degradation rate of PCL-PGS blend electrospun scaffolds was highly dependent on the PGS content [18]. After 21 days under accelerated hydrolytic degradation, coaxial PGS/PCL nanofibers afforded a much higher weight loss (23%) than the residual weight loss verified for monoaxial PCL nanofibers (2.3%). In the first 7 days, a higher degradation rate was observed for the coaxial fibers, possibly due to a fast hydrolytic degradation of the encapsulated PGS. From day 7 onwards, a nearly linear mass loss suggests *in vitro* degradation by surface erosion, which is the predominant mechanism described for both PGS and PCL polymers [49,50]. Previously, Hou et al. reported a weight loss of 26% for coaxial PGS/PCL microfibers after 12 days under accelerated degradation conditions, however, the NaOH solution used was twice as concentrated as the one used in this work [40]. Nevertheless, direct comparisons between different studies are difficult as the degradation is dependent on many factors including scaffold structural features (e.g. fiber diameter) [51].

The integration of chondroinductive factors such as proteins or small molecules with biomimetic electrospun scaffolds appears to be a promising route for improved CTE strategies. Small molecules (e.g. KGN) offer important advantages over protein growth factors, such as high stability and lower cost [52]. KGN has been described as a promising drug for cartilage regeneration *in vivo*. However, after injection, small molecules like KGN are quickly cleared through the lymphatic system, limiting its local effects and compromising its therapeutic effectiveness. Therefore, different drug delivery systems have been recently developed to achieve the sustained and localized delivery of KGN [23–28,53,54]. We speculated that coaxial aligned electropsun nanofibers able to release KGN in a controlled manner would promote hBMSC chondrogenesis, and therefore, promising for improved CTE strategies, particularly for the regeneration of the superficial zone. KGN incorporation did not result in any meaningful change in the structure of the electrospun scaffolds, which is in agreement with a recent study using KGN-encapsulating fibrous membranes to enhance rotator cuff tendon-bone healing [54]. Coaxial PGS-KGN/PCL aligned nanofibers promoted a much more controlled *in vitro* release of KGN than monoaxial PCL-KGN aligned nanofibers. This observation results from the fact that in the coaxial configuration, KGN is confined in the core region of the nanofibers and needs to first disperse through the shell polymer before exits the fiber. In contrast, in the monoaxial PCL-KGN nanofibers, KGN is randomly distributed throughout the nanofiber and possibly located on the fiber surface, which might explain the initial burst release observed.

The bioactivity of the released KGN was assessed through the evaluation of KGN-loaded electrospun scaffolds ability to promote hBMSC growth and chondrogenesis. Both coaxial PGS-KGN/PCL and PCL-KGN aligned nanofibers significantly promoted the proliferation of hBMSC in comparison to non-loaded scaffolds. These results are in agreement with previous studies reporting the enhancing effect of KGN supplementation in hBMSC growth [22,55]. Additionally, Zhu and colleagues reported improved proliferation of human adipose-derived MSC in the presence of KGN delivered from a chitosan-hyaluronic acid hydrogel, which also supports our observations [53]. Importantly, our results demonstrated that after 21 days of differentiation in the absence of TGF-β3, both coaxial/monoaxial KGN-loaded electrospun scaffolds promoted sGAG production and chondrogenic gene expression when compared to the respective non-loaded scaffolds. In agreement, previous studies showed that KGN supplementation either as culture media additive or through nanoparticle-mediated delivery promotes increased sGAG production during the chondrogenic differentiation of hBMSC in micromass cultures without TGF-β3 [25,56]. Regarding the upregulation of chondrogenic markers in hBMSC-seeded KGN-loaded scaffolds, similar trends were observed in previous studies using different KGN-delivery systems combined with human MSC [25,53]. In agreement to our results, Zhu et al. recently reported enhanced expressions of *ACAN*, *COL2* and *Sox9* genes in rat bone MSC cultured in aligned KGN encapsulated PCL membranes in comparison to the membranes without KGN [54]. Moreover, our observations are also supported by the results from Yin et al., which observed significantly increased *Sox9* and *COL2* expressions in rabbit BMSC cultured on KGN-loaded P(LLA-CL)/collagen nanofibrous scaffolds [57].

5. Conclusions

In summary, we have successfully fabricated and characterized coaxial PGS/PCL aligned electrospun scaffolds able to mimic the nanoscale and alignment of collagen fibers present in articular cartilage ECM. The coaxial PGS/PCL aligned nanofibers produced were able to promote a much more sustained release of KGN in comparison to monoaxial PCL aligned scaffolds. Importantly, KGN-loaded aligned nanofiber scaffolds promoted significantly the proliferation and

chondrogenic differentiation of hBMSC, favoring cartilage-like ECM production and gene expression, in the absence of chondrogenic cytokine TGF-β3. Overall, our results highlight the potential of KGN-loaded coaxial aligned nanofibers for the development of novel biomimetic MSC-based strategies to regenerate articular cartilage, particularly for the repair of defects in its superficial zone.

Declaration of competing interest

The authors declare no conflict of interest.

Acknowledgements

Appendix A. Supplementary data

Supplementary data to this article can be found online at https://doi.org/10.1016/j.msec.2019.110291.

Author's contributions

J.C.S and R.J.L. conceived and designed the study. J.C.S., R.N.U, J.C, C.D.M and F.F.F.G. carried out the experimental work. J.C.S. and R.J.L. wrote the manuscript. All the authors participated in the data analysis, reviewing and editing of the final manuscript.

References

[1] T.J. Klein, J. Malda, R.L. Sah, D.W. Hutmacher, Tissue engineering of articular cartilage with biomimetic zones, Tissue Eng. B Rev. 15 (2009) 143–157, https://doi.org/10.1089/ten.teb.2008.0563.

[2] V.C. Mow, X.E. Guo, Mechano-electrochemical properties of articular cartilage: their inhomogeneities and anisotropies, Annu. Rev. Biomed. Eng. 4 (2002) 175–209, https://doi.org/10.1146/annurev.bioeng.4.110701.120309.

[3] E.B. Hunziker, T.M. Quinn, H.-J. Häuselmann, Quantitative structural organization of normal adult human articular cartilage, Osteoarthr. Cartil. 10 (2002) 564–572, https://doi.org/10.1053/joca.2002.0814.

[4] A.G. Mikos, J.S. Temenoff, Review: tissue engineering for regeneration of articular cartilage, Biomaterials 21 (2000) 431–440.

[5] A.R. Poole, What type of cartilage repair are we attempting to attain? J. Bone Jt. Surg. - Ser. A. 85 (2003) 40–44, https://doi.org/10.2106/00004623-200300002-00006.

[6] D.I. Braghirolli, D. Steffens, P. Pranke, Electrospinning for regenerative medicine: a review of the main topics, Drug Discov. Today 19 (2014) 743–753, https://doi.org/10.1016/j.drudis.2014.03.024.

[7] J.K. Wise, A.L. Yarin, C.M. Megaridis, M. Cho, Chondrogenic differentiation of human mesenchymal stem cells on oriented nanofibrous scaffolds: engineering the superficial zone of articular cartilage, Tissue Eng. A 15 (2009) 913–921, https://doi.org/10.1089/ten.tea.2008.0109.

[8] L.E. Sperling, K.P. Reis, P. Pranke, J.H. Wendorff, Advantages and challenges offered by biofunctional core-shell fiber systems for tissue engineering and drug delivery, Drug Discov. Today 21 (2016) 1243–1256, https://doi.org/10.1016/j.drudis.2016.04.024.

[9] B. Pant, M. Park, S.-J. Park, Drug delivery applications of core-sheath nanofibers prepared by coaxial electrospinning: a review, Pharmaceutics 11 (2019) 305, https://doi.org/10.3390/pharmaceutics11070305.

[10] Y. Ding, W. Li, F. Zhang, Z. Liu, N.Z. Ezazi, D. Liu, H.A. Santos, Electrospun fibrous architectures for drug delivery, tissue engineering and cancer therapy, Adv. Funct. Mater. 29 (2019) 1802851, https://doi.org/10.1002/adfm.201802852.

[11] J. Wang, B. Sun, L. Tian, X. He, Q. Gao, T. Wu, S. Ramakrishna, J. Zheng, X. Mo, Evaluation of the potential of rhTGF- β3 encapsulated P(LLA-CL)/collagen nanofibers for tracheal cartilage regeneration using mesenchymal stems cells derived from Wharton's jelly of human umbilical cord, Mater. Sci. Eng. C 70 (2017) 637–645, https://doi.org/10.1016/j.msec.2016.09.044.

[12] C. Wang, W. Hou, X. Guo, J. Li, T. Hu, M. Qiu, S. Liu, X. Mo, X. Liu, Two-phase electrospinning to incorporate growth factors loaded chitosan nanoparticles into electrospun fibrous scaffolds for bioactivity retention and cartilage regeneration, Mater. Sci. Eng. C 79 (2017) 507–515, https://doi.org/10.1016/j.msec.2017.05.075.

[13] Z. Man, L. Yin, Z. Shao, X. Zhang, X. Hu, J. Zhu, L. Dai, H. Huang, L. Yuan, C. Zhou, H. Chen, Y. Ao, The effects of co-delivery of BMSC-affinity peptide and rhTGF-β1 from coaxial electrospun scaffolds on chondrogenic differentiation, Biomaterials 35 (2014) 5250–5260, https://doi.org/10.1016/j.biomaterials.2014.03.031.

[14] Y. Wang, G.A. Ameer, B.J. Sheppard, R. Langer, A tough biodegradable elastomer, Nat. Biotechnol. 20 (2002) 602–606, https://doi.org/10.1038/nbt0602-602.

[15] X.J. Loh, A. Abdul Karim, C. Owh, Poly(glycerol sebacate) biomaterial: synthesis and biomedical applications, J. Mater. Chem. B. 3 (2015) 7641–7651, https://doi.org/10.1039/c5tb01048a.

[16] M.A. Woodruff, D.W. Hutmacher, The return of a forgotten polymer—polycaprolactone in the 21st century, Prog. Polym. Sci. 35 (2010) 1217–1256, https://doi.org/10.1016/j.progpolymsci.2010.04.002.

[17] S.W. Low, Y.J. Ng, T.T. Yeo, N. Chou, Use of Osteoplug polycaprolactone implants as novel burr-hole covers, Singap. Med. J. 50 (2009) (2009) 777–780 50(8): 777-780..

[18] N. Masoumi, B.L. Larson, N. Annabi, M. Kharaziha, B. Zamanian, K.S. Shapero, A.T. Cubberley, G. Camci-Unal, K.B. Manning, J.E. Mayer Jr., A. Khademhosseini, P.G.S. Electrospun, PCL microfibers align human valvular interstitial cells and provide tunable scaffold anisotropy, Adv. Healthc. Mater. 3 (2014) 929–939, https://doi.org/10.1002/adhm.201300505.

[19] L. Vogt, L.R. Rivera, L. Liverani, A. Piegat, M. El Fray, A.R. Boccaccini, Poly(ε-caprolactone)/poly(glycerol sebacate) electrospun scaffolds for cardiac tissue engineering using benign solvents, Mater. Sci. Eng. C 103 (2019) 109712, https://doi.org/10.1016/j.msec.2019.04.091.

[20] S. Salehi, M. Czugala, P. Stafiej, M. Fathi, T. Bahners, J.S. Gutmann, B.B. Singer, T.A. Fuchsluger, Poly (glycerol sebacate)-poly (ε-caprolactone) blend nanofibrous scaffold as intrinsic bio- and immunocompatible system for corneal repair, Acta Biomater. 50 (2017) 370–380, https://doi.org/10.1016/j.actbio.2017.01.013.

[21] Y. Liu, K. Tian, J. Hao, T. Yang, X. Geng, W. Zhang, Biomimetic poly(glycerol sebacate)/polycaprolactone blend scaffolds for cartilage tissue engineering, J. Mater. Sci. Mater. Med. 30 (2019) 53, https://doi.org/10.1007/s10856-019-6257-3.

[22] K. Johnson, S. Zhu, M.S. Tremblay, J.N. Payette, J. Wang, L.C. Bouchez, S. Meeusen, A. Althage, C.Y. Cho, X. Wu, P.G. Schultz, A stem cell-based approach to cartilage repair, Science 336 (2012) 717–721, https://doi.org/10.1126/science.1215157.

[23] G. Cai, W. Liu, Y. He, J. Huang, L. Duan, J. Xiong, L. Liu, D. Wang, Recent advances in kartogenin for cartilage regeneration, J. Drug Target. 27 (2019) 28–32, https://doi.org/10.1080/1061186X.2018.1464011.

[24] Q. Hu, B. Ding, X. Yan, L. Peng, J. Duan, S. Yang, L. Cheng, D. Chen, Polyethylene glycol modified PAMAM dendrimer delivery of kartogenin to induce chondrogenic differentiation of mesenchymal stem cells, Nanomed. Nanotechnol. Biol. Med. 13 (2017) 2189–2198, https://doi.org/10.1016/j.nano.2017.05.011.

[25] M.L. Kang, J.Y. Ko, J.E. Kim, G. Il Im, Intra-articular delivery of kartogenin-conjugated chitosan nano/microparticles for cartilage regeneration, Biomaterials 35 (2014) 9984–9994, https://doi.org/10.1016/j.biomaterials.2014.08.042.

[26] W. Fan, J. Li, L. Yuan, J. Chen, Z. Wang, Y. Wang, C. Guo, X. Mo, Z. Yan, Intra-articular injection of kartogenin-conjugated polyurethane nanoparticles attenuates the progression of osteoarthritis, Drug Deliv. 25 (2018) 1004–1012, https://doi.org/10.1080/10717544.2018.1461279.

[27] D. Shi, X. Xu, Y. Ye, K. Song, Y. Cheng, J. Di, Q. Hu, J. Li, H. Ju, Q. Jiang, Z. Gu, Photo-cross-linked scaffold with kartogenin-encapsulated nanoparticles for cartilage regeneration, ACS Nano 10 (2016) 1292–1299, https://doi.org/10.1021/acsnano.5b06663.

[28] X. Li, J. Ding, Z.-Z. Zhang, M. Yang, J.-K. Yu, J.C. Wang, F. Chang, X. Chen, Kartogenin-incorporated thermogel supports stem cells for significant cartilage regeneration, ACS Appl. Mater. Interfaces 8 (2016) 5148–5159, https://doi.org/10.1021/acsami.5b12212.

[29] L. Zheng, D. Li, W. Wang, Q. Zhang, X. Zhou, D. Liu, J. Zhang, Z. You, J. Zhang, C. He, Bilayered scaffold prepared from kartogenin loaded hydrogel and BMP-2-derived peptides loaded porous nanofibrous scaffold for osteochondral defect repair, ACS Biomater. Sci. Eng. 5 (2019) 4564–4573, https://doi.org/10.1021/acsbiomaterials.9b00513.

[30] W. Yang, Y. Zheng, J. Chen, Q. Zhu, L. Feng, Y. Lan, P. Zhu, S. Tang, R. Guo, Preparation and characterization of the collagen/cellulose nanocrystals/USPIO scaffolds loaded kartogenin for cartilage regeneration, Mater. Sci. Eng. C 99 (2019) 1362–1373, https://doi.org/10.1016/j.msec.2019.02.071.

[31] R. Rai, M. Tallawi, N. Barbani, C. Frati, D. Madeddu, S. Cavalli, G. Graiani, F. Quaini, J.A. Roether, D.W. Schubert, E. Rosellini, A.R. Boccaccini, Biomimetic poly(glycerol sebacate) (PGS) membranes for cardiac patch application, Mater. Sci. Eng. C 33 (2013) 3677–3687, https://doi.org/10.1016/j.msec.2013.04.058.

[32] L. Hou, W.M.R.N. Udangawa, A. Pochiraju, W. Dong, Y. Zheng, R.J. Linhardt, T.J. Simmons, Synthesis of heparin-immobilized, magnetically addressable cellulose nanofibers for biomedical applications, ACS Biomater. Sci. Eng. 2 (2016) 1905–1913, https://doi.org/10.1021/acsbiomaterials.6b00273.

[33] A. Shafiee, M. Soleimani, G.A. Chamheidari, E. Seyedjafari, M. Dodel, A. Atashi, Y. Gheisari, Electrospun nanofiber-based regeneration of cartilage enhanced by mesenchymal stem cells, J. Biomed. Mater. Res. A 99A (2011) 467–478, https://doi.org/10.1002/jbm.a.33206.

[34] J.W. Reboredo, T. Weigel, A. Steinert, L. Rackwitz, M. Rudert, H. Walles, Investigation of migration and differentiation of human mesenchymal stem cells on five-layered collagenous electrospun scaffold mimicking native cartilage structure, Adv. Healthc. Mater. 5 (2016) 2191–2198, https://doi.org/10.1002/adhm.201600134.

[35] M.L. Alves Da Silva, A. Martins, A.R. Costa-Pinto, P.F. Costa, S. Faria, M.E. Gomes, R.L. Reis, N.M. Neves, Cartilage tissue engineering using electrospun PCL nanofiber meshes and MSCs, Biomacromolecules 11 (2010) 3228–3236, https://doi.org/10.1021/bm100476r.

[36] A. Cheng, Z. Schwartz, A. Kahn, X. Li, Z. Shao, M. Sun, Y. Ao, B.D. Boyan, H. Chen, Advances in porous scaffold design for bone and cartilage tissue engineering and regeneration, Tissue Eng. B Rev. 25 (2019) 14–29, https://doi.org/10.1089/ten.teb.2018.0119.

[37] J.L. Ifkovits, R.F. Padera, J.A. Burdick, Biodegradable and radically polymerized elastomers with enhanced processing capabilities, Biomed. Mater. 3 (2008) 034104, , https://doi.org/10.1088/1748-6041/3/3/034104.

[38] M. Kharaziha, M. Nikkhah, S.R. Shin, N. Annabi, N. Masoumi, A.K. Gaharwar, G. Camci-Unal, A. Khademhosseini, PGS:Gelatin nanofibrous scaffolds with tunable mechanical and structural properties for engineering cardiac tissues, Biomaterials 34 (2013) 6355–6366, https://doi.org/10.1016/j.biomaterials.2013.04.045.

[39] S. Sant, C.M. Hwang, S.-H. Lee, A. Khademhosseini, Hybrid PGS–PCL microfibrous scaffolds with improved mechanical and biological properties, J. Tissue Eng. Regenerat. Med. 5 (2011) 283–291, https://doi.org/10.1002/term.

[40] L. Hou, X. Zhang, P.E. Mikael, L. Lin, W. Dong, Y. Zheng, T.J. Simmons, F. Zhang, R.J. Linhardt, Biodegradable and Bioactive PCL-PGS core-shell fibers for tissue engineering, ACS Omega 2 (2017) 6321–6328, https://doi.org/10.1021/acsomega.7b00460.

[41] F. Yi, D.A. La Van, Poly(glycerol sebacate) nanofiber scaffolds by core/shell electrospinning, Macromol. Biosci. 8 (2008) 803–806, https://doi.org/10.1002/mabi.200800041.

[42] H.J. Wu, M.H. Hu, H.Y. Tuan-Mu, J.J. Hu, Preparation of aligned poly(glycerol sebacate) fibrous membranes for anisotropic tissue engineering, Mater. Sci. Eng. C 100 (2019) 30–37, https://doi.org/10.1016/j.msec.2019.02.098.

[43] J.C. Schagemann, S. Paul, M.E. Casper, J. Rohwedel, J. Kramer, C. Kaps, H. Mittelstaedt, M. Fehr, G.G. Reinholz, Chondrogenic differentiation of bone marrow-derived mesenchymal stromal cells via biomimetic and bioactive poly-ε-caprolactone scaffolds, J. Biomed. Mater. Res. A 101 (2013) 1620–1628, https://stem.doi.org/10.1002/jbm.a.34457.

[44] A.K. Gaharwar, M. Nikkhah, S. Sant, A. Khademhosseini, Anisotropic poly (glycerol sebacate)-poly (-caprolactone) electrospun fibers promote endothelial cell guidance, Biofabrication 7 (2014) 015001, , https://doi.org/10.1088/1758-5090/7/1/015001.

[45] S. Salehi, M. Fathi, S.H. Javanmard, T. Bahners, J.S. Gutmann, S. Ergün, K.P. Steuhl, T.A. Fuchsluger, Generation of PGS/PCL blend nanofibrous scaffolds mimicking corneal stroma structure, Macromol. Mater. Eng. 299 (2014) 455–469, https://doi.org/10.1002/mame.201300187.

[46] G.H. Kim, Electrospun PCL nanofibers with anisotropic mechanical properties as a biomedical scaffold, Biomed. Mater. 3 (2008) 025010, , https://doi.org/10.1088/1748-6041/3/2/025010.

[47] H. Sun, L. Mei, C. Song, X. Cui, P. Wang, The in vivo degradation, absorption and excretion of PCL-based implant, Biomaterials 27 (2006) 1735–1740, https://doi.org/10.1016/j.biomaterials.2005.09.019.

[48] Y. Wang, Y.M. Kim, R. Langer, In vivo degradation characteristics of poly (glycerol sebacate), J. Chem. Phys. 66 (2003) 192–197, https://doi.org/10.1063/1.1733007.

[49] I. Pomerantseva, N. Krebs, A. Hart, C.M. Neville, A.Y. Huang, C.A. Sundback, Degradation behavior of poly(glycerol sebacate), J. Biomed. Mater. Res. A 91A (2009) 1038–1047, https://doi.org/10.1002/jbm.a.32327.

[50] M. Bartnikowski, T.R. Dargaville, S. Ivanovski, D.W. Hutmacher, Degradation mechanisms of polycaprolactone in the context of chemistry, geometry and environment, Prog. Polym. Sci. 96 (2019) 1–20, https://doi.org/10.1016/j.progpolymsci.2019.05.004.

[51] Y. You, B.M. Min, S.J. Lee, T.S. Lee, W.H. Park, In vitro degradation behavior of electrospun polyglycolide, polylactide, and poly(lactide-co-glycolide), J. Appl. Polym. Sci. 95 (2004) 193–200, https://doi.org/10.1002/app.21116.

[52] K.W. Lo, T. Jiang, K.A. Gagnon, C. Nelson, C.T. Laurencin, Small-molecule based musculoskeletal regenerative engineering, Trends Biotechnol. 32 (2014) 74–81, https://doi.org/10.1016/j.tibtech.2013.12.002.

[53] Y. Zhu, J. Tan, H. Zhu, G. Lin, F. Yin, L. Wang, K. Song, Y. Wang, G. Zhou, W. Yi, Development of kartogenin-conjugated chitosan-hyaluronic acid hydrogel for nucleus pulposus regeneration, Biomater. Sci. 5 (2017) 784–791, https://doi.org/10.1039/c7bm00001d.

[54] Q. Zhu, Z. Ma, H. Li, H. Wang, Y. He, Enhancement of rotator cuff tendon-bone healing using combined aligned electrospun fibrous membranes and kartogenin, RSC Adv. 9 (2019) 15582–15592, https://doi.org/10.1039/c8ra09849b.

[55] T. Spakova, J. Plsikova, D. Harvanova, M. Lacko, S. Stolfa, J. Rosocha, Influence of kartogenin on chondrogenic differentiation of human bone Marrow-Derived MSCs in 2D culture and in Co-Cultivation with OA osteochondral explant, Molecules 23 (2018) 1–16, https://doi.org/10.3390/molecules23010181.

[56] J. Xu, J. Li, S. Lin, T. Wu, H. Huang, K. Zhang, Y. Sun, K.W.K. Yeung, G. Li, L. Bian, Nanocarrier-mediated codelivery of small molecular drugs and siRNA to enhance chondrogenic differentiation and suppress hypertrophy of human mesenchymal stem cells, Adv. Funct. Mater. 26 (2016) 2463–2472, https://doi.org/10.1002/adfm.201504070.

[57] H. Yin, J. Wang, Z. Gu, W. Feng, M. Gao, Y. Wu, H. Zheng, X. He, X. Mo, Evaluation of the potential of kartogenin encapsulated poly(L-lactic acid-co-caprolactone)/collagen nanofibers for tracheal cartilage regeneration, J. Biomater. Appl. 32 (2017) 331–341, https://doi.org/10.1177/0885328217717077.